BBA - Biomembranes 1863 (2021) 183571

Contents lists available at ScienceDirect

BBA - Biomembranes

journal homepage: www.elsevier.com/locate/bbamem

Lipid domain formation and non-lamellar structures associated with varied lysylphosphatidylglycerol analogue content in a model Staphylococcal plasma membrane

Reg Rehal [a], Robert D. Barker [b], Zidong Lu [a,1], Tam T. Bui [c], Bruno Demé [d], Gerd Hause [e], Christian Wölk [f,*], Richard D. Harvey [g,*]

[a] School of Cancer and Pharmaceutical Sciences, King's College London, UK
[b] School of Physical Sciences, University of Kent, Canterbury, UK
[c] Biomolecular Spectroscopy Centre, King's College London, UK
[d] Institut Laue Langevin, 71 avenue des Martyrs, CS 20156, 38042 Grenoble, France
[e] Biozentrum, Martin-Luther-Universität Halle-Wittenberg, Halle (Saale), Germany
[f] Institute of Pharmacy, Leipzig University, Eilenburger Straße 15a, 04317 Leipzig, Germany
[g] Department of Pharmaceutical Chemistry, University of Vienna, Althanstraße 14, A-1090 Vienna, Austria

ARTICLE INFO

Keywords:
Lysylphosphatidylglycerol
Lipid-lipid complexes
Polymorphism
Membrane domains
Antibiotic resistance

ABSTRACT

Dipalmitoyl-3-aza-dehydroxy-lysylphosphatidylglycerol (DP3adLPG), is a chemically stable synthetic analogue of the bacterial lipid lysylphosphatidylglycerol (LPG), designed as a substitute for the notoriously labile native lipid in biophysical investigations. In *Staphylococcus aureus*, LPG is known to play a role in resistance to antibiotics by altering membrane charge properties in response to environmental stress, but little is known about how LPG influences other bilayer physicochemical properties or lateral organisation, through the formation of complexes with lipids such as phosphatidylglycerol (PG). In this study we have investigated the different phases formed by biomimetic mixtures of 3adLPG and PG in different thermotropic states, using neutron diffraction and electron microscopy. In a DPPG/DP3adLPG 70:30 mol% mixture, two distinct lamellar phases were observed below the lipid melting transition: $L_{\beta'}$ 1 and $L_{\beta'}$ 2 with respective periodicities of 82 and 62 Å. Increasing the proportion of DP3adLPG to mimic the effects of environmental stress led to the disappearance of the $L_{\beta'}$ 1 phase and the formation of an inverse hexagonal phase. The compositions of these different phases were identified by investigating the thermotropic properties of the two mixtures, and probing their interaction with the antimicrobial peptide magainin 2 F5W. We propose that the observed polymorphism results from the preferential formation of either triplet PG-3adLPG-PG, or paired PG-3adLPG complexes, dependent upon the mixing proportions of the two lipids. The relevance of these findings to the role native LPG in *S. aureus*, are discussed with respect to their influence on antibiotic resistance and lateral membrane organisation.

1. Introduction

The role played by the aminoacyl lipid lysylphosphatidylglycerol (LPG) (Fig. 1A) in resistance to host defensive cationic antimicrobial peptides (CAPs) in *Staphylococcus aureus* and other Gram positive bacteria, has been elucidated mostly through in vitro genotypic and phenotypic studies. Detection of CAPs via the antimicrobial peptide sensing system (*aps*) [1] leads to increased biosynthesis of LPG, and its membrane translocation, via the dual-function lysyl-transferase/flippase MprF [2]. Thus the LPG present in the *S. aureus* plasma membrane outer leaflet is thought to provide an increase in "net positive charge" which effects repulsion of cationic antimicrobials and thus inhibits their membrane activity [3]. This simplistic view envisages LPG as providing discrete points of positive charge within a matrix of predominantly anionic phospholipids (phosphatidylglycerol – PG and cardiolipin - CL) [4], without acknowledging the fact that LPG readily forms ion-pairs

* Corresponding authors.
E-mail addresses: Christian.Woelk@medizin.uni-leipzig.de (C. Wölk), richard.harvey@univie.ac.at (R.D. Harvey).
[1] Current affiliation: National Engineering Research Centre for Tissue Restoration and Reconstruction, South China University of Technology, Guangzhou, Guangdong, China.

https://doi.org/10.1016/j.bbamem.2021.183571
Received 13 November 2020; Received in revised form 25 January 2021; Accepted 29 January 2021
Available online 6 February 2021

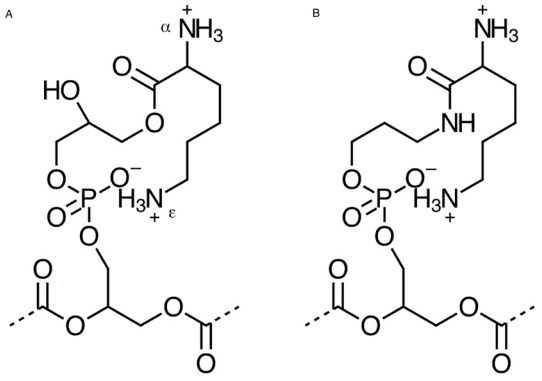

Fig. 1. Headgroup structures of A) native lysylphosphatidylglycerol (with labelled α and ε amines) and B) synthetic 3-aza-dehydroxy lysylphosphatidylglycerol (3adLPG).

with PG, which act as discrete complexes with an overall neutral charge [5,6]. Since the proportion of LPG present in the membrane outer leaflet has rarely been shown to exceed 30% of the total phospholipids, even in resistant phenotypes [2,3,7–9], it must be assumed to be fully sequestered into ion pairs by the more abundant PG, thus contributing to an overall charge dampening of the plasma membrane [10], when symmetrically distributed between the bilayer leaflets [3]. In this more nuanced picture of the role of LPG in membrane defence, it is increased neutralisation of PG which facilitates CAP resistance and not the cumulative effect of discrete regions of charge inversion.

Synthetic L-PG has previously been used in model *S. aureus* membranes to study their interaction with AMPs. The findings of these studies have suggested that the presence of LPG does not inhibit peptide binding, but rather impedes their penetration into lipid bilayers [11]. Unequivocal interpretation of these results is extremely problematic, however, since LPG has a highly labile ester in its headgroup, which is readily hydrolysed at neutral pH [12]. In order to avoid the problem of LPG hydrolysis during biophysical investigations into its effect on membrane behaviour and AMP interaction, one approach has been to synthesise a stable analogue in the form of lysylphosphatidylethanolamine (LPE) [13]. Although increasing proportions of LPE were found to attenuate the membrane lytic effect of AMPs in vesicles containing PG and phosphatidylcholine (PC), increasing the PC content alone exhibited the same effect [13]. This seems to suggest that the LPE behaves more like a zwitterionic lipid such as PC when incorporated into PG-containing bilayers, however this is not that case with native L-PG, which carries a net +1 charge under mildly acidic conditions such as those present at the outer leaflet of the *S. aureus* plasma membrane [10,14]. The relevance of using LPE as a substitute for LPG is therefore dependent upon the pH at which experiments were conducted (pH 7.5) [13] and the pK_a of its α amine, which in the case of native LPG (Fig. 1A) is ~6.5 [15]. It follows that in pH neutral environments, LPG would indeed be predominantly zwitterionic, and therefore studying its bilayer stabilising or AMP-repelling effects under these conditions would not yield sufficiently biorelevant results.

A second synthetic stable analogue of L-PG, named 1,2-*O*-dipalmitoyl-3-aza-dehydroxy lysyl-phosphatidylglycerol (DP3adLPG) (Fig. 1B), has been shown to stabilize fluid bilayers in binary mixtures with PG and attenuate AMP penetration, when fully ionized under mild acidic conditions [16]. In monolayer studies, DP3adLPG was found to mix ideally with PG, potentially forming both discrete neutral ion pairs and putative DPPG-DP3adLPG-DPPG ion triplets, with a net negative charge [6]. It could therefore be argued, that studying the effects of LPG and its analogues in model bacterial membranes, should really focus on the lipid ion pair or indeed ion triplet as a discrete entity, rather than focusing on the behaviour of the individual lipids. With respect to this concept, the ion pairs formed between DP3adLPG and DPPG may therefore serve as useful substitutes for the complexes formed between native LPG and PG [5], when it comes to assessing their role in modifying membrane behaviour using biophysical experiments.

In this study we have examined the thermotropic and self-association phase behaviour of biomimetic mixtures of DP3adLPG and DPPG, using a combination of neutron diffraction, differential scanning calorimetry and electron microscopy techniques. Our focus has been on two DPPG/DP3adLPG mixtures, with molar ratios of 70:30 and 45:55, to mimic the proportions found in virulent methicillin resistant *S. aureus* (MRSA) ST239 TW strain [17], when grown respectively in mild conditions and under acidic stress [10,16]. Although the phase behaviour detectable using these techniques may exhibit differences based on the limitations of sample preparation, such as alterations in solvent concentration, the higher pK_a of DP3adLPG (~8.15) [6] compared to native L-PG, should ensure the formation of ion pairs over a wide range of solvent conditions. One AMP, magainin 2 F5W, has been used as a probe to assess peptide influence on lipid phase behaviour, to allow discussion of the results in the context of previous studies examining the effect of LPG and its analogues on AMP resistance.

2. Materials and methods

2.1. Materials

Tris(hydroxymethyl)aminomethane (>99.0%), concentrated hydrochloric acid (38%), concentrated deuterium chloride (99%D atom), glacial acetic acid, sodium sulphate (>99.0%) and deuterium oxide (99.9%D atom) were all purchased from Sigma-Aldrich (Gillingham, Dorset, UK) and were used as supplied. The peptide magainin 2 F5W (GIGKWLHSAKKFGKAFVGEIMNS – M_w 2506 Da) (>95%) was custom synthesized by GenScript (Piscataway, New Jersey, USA) and was used as supplied. The phospholipids 1,2-dipalmitoyl-*sn*-glycero-3-phosphocholine (DPPC) (M_w 734.04 Da) and 1,2-dipalmitoyl-*sn*-glycero-3-phospho-(1′-*rac*-glycerol) (DPPG) sodium salt (M_w 744.95 Da), were purchased from Avanti Polar Lipids (Alabaster, AL, USA), and 1,2-dipalmitoyl-3-aza-dehydroxy-lysyl-phosphatidylglycerol (DP3adLPG) trifluoroacetate salt (M_w 963.02 Da) was synthesized at the Institute of Pharmaceutical Science, King's College London, using the method described by Rehal et al. 2019 [16]. For the neutron diffraction studies, the chain-deuterated phospholipids d_{62}1,2-dipalmitoyl-*sn*-glycero-3-phospho-(1′-*rac*-glycerol), (d_{62}DPPG) triethylammonium salt (M_w 886.54 Da) and d_{62}-1,2-dipalmitoyl-3-aza-dehydroxy-lysyl-phosphatidylglycerol (d_{62}DP3adLPG) trifluoroacetate salt (M_w 1025.02 Da) were synthesized at the Institute of Pharmaceutical Science, King's College London [18]. Cleaning solvents; chloroform (99.5%), methanol (99.9%) and acetone (99.9%) were also purchased from Sigma-Aldrich (Chesnes, France) and were used as supplied.

2.2. Methods

2.2.1. Spectroscopic studies of peptide folding and binding

2.2.1.1. Circular dichroism. Liposomes were prepared using DPPG/DP3adLPG mixtures in 70:30, 60:40, 55:45, 40:60 and 30:70 molar ratios. Thin lipid films were prepared in 7 mL capacity glass Bijou bottles by dissolving the lipid mixtures (10 mg total lipid) in chloroform/methanol (9:1 v/v) solvent, prior to rotary evaporation (RE-111, Buchi, Switzerland) under reduced pressure and overnight storage under vacuum in order to ensure removal of residual organic solvent. The lipid films were solvated with 70 mM Tris-HCl pH 7.4 buffer (made using 18.2 MΩ.cm resistivity ultrapure water - Milli-Q 16, Merck Millipore, Billerica, USA), by thorough vortexing followed by 10 min probe sonication (Soniprobe, Lucas Dawe Ultrasonics, UK), to produce optically-clear ~5 mM liposome dispersions. The liposomes were diluted and mixed with solutions of magainin 2 F5W to give final concentrations of

200 μM lipid and 10 μM peptide in 70 mM Tris-HCl buffer. The vesicle/peptide mixed samples were loaded into 2 mm pathlength quartz cells prior to circular dichroism (CD) measurements.

Static far-UV CD measurements (190 nm to 260 nm) were carried out on a Chirascan-Plus spectrometer (Applied Photophysics Ltd., Leatherhead, UK) with a bandwidth of 2 nm scanning at a speed of 1.5 s time per point at 22 °C. The recorded CD spectra were subtracted from those obtained from corresponding peptide-free samples. Ellipticity data was then converted from millidegrees to mean residue (mean $M_w = 113$ Da) ellipticity ($M^{-1}.cm^{-1}$), smoothed using a Savitsky-Golay filter and analysed for different peptide secondary structure content using the Principle Component Regression method based on 16 known protein structures embedded in the PLSPlus/IQ routine on GRAMS32 AI software (Galactic, USA) [19].

2.2.1.2. Tryptophan fluorescence. Liposomes composed of various DPPG/DP3adLPG mixtures (and additionally one DPPC/DPPG [75:25] mixture) were prepared in 70 mM Tris-HCl pH 7.4 buffer as described above. The resultant dispersions were diluted and mixed with solutions of magainin 2 F5W to give final concentrations of 200 μM lipid and 10 μM peptide in 70 mM Tris-HCl buffer to give a lipid/peptide molar ratio of 20:1. Samples were loaded into 10 × 4 mm clear-sided quartz cells and tryptophan fluoresce emission spectra were scanned between 300 and 500 nm following excitation at 280 nm, using a Varian Cary Eclipse fluorescence spectrophotometer (Aligent Technologies, Stockport, UK) at 25 °C with excitation and emission bandwidths of 1 nm. Background spectra obtained from buffer only, were subtracts from all the sample spectra.

In order to avoid the emission intensity distorting effects of liposome-induced light scattering on the fluorescence spectra, their intensities were normalised to give a maximum of 1. The relative degree of peptide binding to the liposomes was calculated from the normalised fluorescence intensities obtained at 320 nm (I_{320}) [20]. It was assumed that the I_{320} obtained for magainin 2 F5W in buffer alone represented 0% binding, and that obtained for the peptide mixed with DPPC/DPPG [75:25] liposomes represented 100% binding.

2.2.2. Differential scanning calorimetry

Liposome dispersions (2 mg mL^{-1}), were produced by the thin film solvation method in ultrapure water, as outlined above (Section 2.2.1), using DPPG/DP3adLPG mixtures with molar ratios of 70:30 and 45:55 and the individual pure lipid components. After formation of dry lipid films, they were incubated in sterile filtered dispersion medium (100 mM NaCl solution) at 60 °C while shaking (1400 rpm) for 30 min. The lipid dispersions formed, were bath sonicated at 37 kHz (100% power output) for 6 min.

The DSC measurements of the lipid dispersions were performed on a MicroCal VP-DSC (MicroCal Inc., Northampton, MA, USA). The scanned temperature range was between 2 and 60 °C, the heating rate was 60 K h^{-1}, and each heating and cooling scan was repeated 3 times to reproduce the number of temperature cycles used during the neutron diffraction measurements. The reference cell was filled with pure solvent, and the buffer–buffer baseline was subtracted from the thermograms of the vesicle samples. The DSC scans were analysed using MicroCal Origin 8.0 software, with the transition temperature (T_m) assigned as the peak maximum, FWHM as the width of the transition peak at half height of the maximum, and ΔH (transition enthalpy) as the integral of the peak.

2.2.3. Neutron diffraction measurements

Orientated multilayers of 20 mg total lipid mixtures of d_{62}DPPG/d_{62}3adPG at molar ratios of 70:30 and 45:55 in the absence and presence of 2 mol% magainin 2 F5W, were prepared by depositing the lipids or lipid/peptide mixtures onto the polished faces of pre-cleaned 50.8 ± 0.50 mm diameter (19.6 cm^2), 275 ± 20 μm thick silicon wafers (Silicon Materials, Kaufering, Germany) from 1 mL chloroform solutions. An even coating of lipids was achieved by allowing an initial solvent evaporation in air while the silicon wafers were clamped horizontally. Residual solvent was removed from the air-dried samples by keeping them under vacuum for 12 h. The coated silicon wafers were annealed by placing them over a saturated Na_2SO_4 bath for 24 h at 50 °C in a hermetically-sealed vessel to achieve 85% humidity.

After annealing, each lipid-coated silicon wafer was mounted onto a goniometer sealed within a temperature-controlled aluminium chamber, which contained an internal solvent reservoir. The relative humidity within the sample chamber was maintained at approximately 100% by ensuring that the temperature solvating H_2O or D_2O matched that of the atmosphere surrounding the sample [21], by heating both with water circulating from thermal baths maintained at either 25 °C or 55 °C (ensuring that the lipids were in the gel or fluid phases respectively).

Neutron diffraction measurements were performed on the D16 diffractometer at the Institut Laue-Langevin (Grenoble, France) using a λ = 4.762 Å incident neutron beam with a 1% spread focused at the sample position by a pyrolitic graphite monochromator, with a fixed detector distance of 1 m. Neutron diffraction profiles (Intensity versus 2θ) were compiled for each sample by performing θ scans in steps of 0.05° (where θ is the sample angle) at various fixed detector positions.

For each d_{62}DPPG/d_{62}3adPG sample either with or without magainin 2 F5W, neutron diffraction was first measured with H_2O vapour solvation at 25 °C before increasing the temperature to 55 °C for a second diffraction measurement. Samples were allowed to cool again to 25 °C, before solvation with D_2O vapour for the third measurement and then heated to 55 °C for the fourth measurement. This cooling/heating cycle was repeated a third time using H_2O/D_2O 1:1 v/v vapour for solvation.

2.2.3.1. Bragg peak integration. The diffraction intensity (I) profiles obtained for each sample, were recorded as a function of the scattering angle (2θ), and are presented as a function of the scattering vector (q), where $q = (4.\pi.\sin\theta)/\lambda$ ($Å^{-1}$). For the purposes of Bragg peak analysis, the diffraction profiles were plotted as I versus θ using OriginPro® 2016 (OriginLab Corporation, Northampton, MA, USA). Individual peaks and peak clusters were fitted using a Voigt area function after subtraction of a linear baseline created from manually-selected anchor points, in order to obtain the position of the peak maximum (θ) and its integrated intensity (I_h). For lamellar phases which are identifiable by regular spacing of the different Bragg reflection orders (h), the peak maxima are related to the repeat distance (in angstroms) of the one-dimensional unit cell of a stack of bilayers (the sum of the bilayer thickness of one bilayer and the solvent layer separating it from one neighbouring bilayer), known as the d-spacing; such that $d = (\lambda/2\sin\theta).h$, where θ is measured in radians. The relation between d and the scattering vector for a specific diffraction order (q_h) is given by $d = 2.\pi.h/q_h$. In order to compensate for the small variations in the d-spacing obtained from individual q_h values, plots of q versus h (see Supporting information Fig. S1) were used to obtain the d-spacing used for all subsequent analysis, using $d = 2\pi/s$, where s is the slope of the linear regression line.

For non-lamellar phases, the methods by which Bragg peak position maxima were used to index them as either two-dimensional hexagonal phase unit cells (d_{hk}) or three-dimensional cubic phase unit cells (d_{hkl}), are described in detail below.

2.2.3.2. Lamellar phase data analysis. The integrated intensity (I_h) of each Bragg peak of a specific diffraction order in the identifiable lamellar phases, was used to calculate their structure factor amplitude $|F_h|$, using Eq. (1) [22]. This is the first step towards the construction of the one-dimensional bilayer scattering length density (SLD) profile through the unit cell.

$$|F_h| = A_h\sqrt{L.I_h} \quad (1)$$

Since in our analysis the Bragg peak intensities were integrated in θ, the Lorentz correction factor (L) is sin2θ [23]. The sample absorption correction factor (A_h) was calculated using the following formula [24]:

$$A_h = \frac{sin\vartheta}{2.\mu.l}\left(1 - e^{\frac{-2.\mu.l}{sin\vartheta}}\right) \quad (2)$$

In this equation, μ is the beamline wavelength-dependent linear attenuation coefficient and l is the thickness of the solvated lipid film deposited onto the silicon wafer (~12.2 μm). The μ values for the different samples were calculated using an online macro available from the NIST Centre for Neutron Research (https://www.ncnr.nist.gov/instruments/bt1/neutron.html), [25] from densities estimated for the d_{62}DPPG/d_{62}DP3adLPG mixtures (see Supporting information Table S1).

After determining structure factors, an SLD profile through the bilayer in real space perpendicular to the bilayer plane $\rho_s(z)$, was constructed using Fourier synthesis [26]:

$$\rho_s(z) = \frac{2}{d}\sum_{h=1}^{h_{max}} \pm F_h \cdot cos\left(\frac{2.\pi.h.z}{d}\right) \quad (3)$$

Here h is the diffraction order, d is the d-spacing and z is the distance (in angstroms) along the axis perpendicular to the bilayer plane, which can be positive or negative since the SLD profile is centrosymmetric around the mid-point of the unit cell (which may the taken to be either the bilayer centre, or that of the solvent layer). The structure factor may also be of either positive or negative phase, the sign of which needs to be determined in order to complete the Fourier reconstruction. This is achieved by plotting F_h against the fraction of D_2O in the solvent contrast for each of the Bragg peak orders, and manipulating the phase of each F_h in order to produce the best linear fit (see Supporting information Figs. S2 and S3). The direction of slope for each plot is thus informs the pattern of assigned structure factor phases for the specific solvent contrasts using Eq. (3). For the H_2O contrast, the F_h phases required to construct an SLD profile centrosymmetric around the positive SLD bilayer mid-point (due to the deuterated acyl chains), with negative SLD solvent peaks, is + − + + + + for the maximum of six Bragg peak orders measured.

The relative SLD profiles for the H_2O contrasts obtained using Eq. (3), were normalised so that the solvent minima were fixed at -0.56×10^{-6} Å^{-2} and the bilayer centre maxima were fixed at the theoretical SLD values for the relevant lipid mixtures (either 5.98×10^{-6} Å^{-2} for the d_{62}DPPG/d_{62}DP3adLPG 70:30 mixture, or 5.84×10^{-6} Å^{-2} for the 45:55 mixture).

2.2.3.3. Non-lamellar phase data analysis. In addition to the lamellar phases, with their characteristic 1:2:3:4 etc. Bragg peak position ratios, the neutron diffraction patterns were also analysed for the presence of non-lamellar phases. For inverse hexagonal phase (H_{II}), characterised by lipids surrounding rod-shaped solvent cores packed into hexagonal lattices [27], the positions of the Bragg peaks are described by the function:

$$q_{hk} = \frac{4\pi}{\sqrt{3}.a}\cdot\sqrt{h^2 + k^2 + hk} \quad (4)$$

where a is the repeat distance from the centre of one solvent rod to an adjacent one, known as the lattice constant, and h, k are the Miller indices. The ratios of the Bragg peak positions in an H_{II} phase are characteristically $1:\sqrt{3}:2:\sqrt{7}:3:\sqrt{12}:\sqrt{13}:4$ etc. [28].

The Bragg peak positions of bicontinuous cubic phases occur at:

$$q_{hkl} = \frac{2\pi}{a}\cdot\sqrt{h^2 + k^2 + l^2} \quad (5)$$

where a is the lattice constant and h, k, l are the Miller indices [28]. The ratios of the Bragg peak positions in cubic phases are dependent upon their geometric symmetry [29].

2.2.4. Cryo transmission electron microscopy

Liposome dispersions (2 mg mL^{-1}) were prepared using the thin film rehydration procedure as stated above (2.2.1) 100 mM NaCl solution was added for film hydration. The lipid formulations were incubated at 50 °C while shaking (1400 rpm, 30 min), followed by bath sonication (37 kHz, 50 °C, 3 min).

Vitrified specimens were prepared using a blotting procedure, performed in a chamber with controlled temperature and humidity using an EM GP grid plunger (Leica, Wetzlar, Germany). The sample dispersion (6 μL) was placed onto an EM grid coated with a holey carbon film (C^{flat}, Protochips Inc., Raleigh, NC). Excess solution was then removed by blotting with a filter paper to leave a thin film of the dispersion spanning the holes of the carbon film on the EM grid. Vitrification of the thin film was achieved by rapid plunging of the grid into liquid ethane held just above its freezing point. The vitrified specimen was kept below 108 K during storage, transferred to the microscope and investigated. Specimens were examined with a Libra 120 Plus transmission electron microscope (Carl Zeiss Microscopy GmbH, Oberkochen, Germany), operating at 120 kV. The microscope was equipped with a Gatan 626 cryotransfer system. Images were acquired using a BM-2 k-120 dual-speed on-axis SSCCD camera (TRS, Moorenweis, Germany).

2.2.5. Freeze-fracture electron microscopy

Liposome dispersions (4 mg mL^{-1}), were produced by the thin film solvation method in ultrapure water, as outlined above (Section 2.2.2), using DPPG/DP3adLPG mixtures with molar ratios of 70:30 and 45:55. An ultasonicator bath (Sonorex super, Berlin, Germany) with a power of 320 W and a frequency of 35 kHz, was used to sonicate the liposomes at 50 °C for 1 h, to obtain translucent dispersions.

For freeze fracture analysis, the liposome samples were fixed using propane jet-freeze device JFD 030 (BAL-TEC, Balzers, Liechtenstein). Afterwards, the samples were freeze-fractured at −150 °C without etching with a freeze-fracture/freeze etching system BAF 060 (BAL-TEC, Balzers, Liechtenstein). The surfaces were shadowed with platinum (2 nm layer, shadowing angle 45°) and subsequently with carbon (20 nm layer, shadowing angle 90°). The replicas were floated into a sodium chloride solution (4% available chlorine) for 30 min, rinsed in distilled water for 10 min, then washed in 30% acetone for 30 min and finally rinsed in distilled water for 10 min. Thereafter, the replicas were mounted on copper grids coated with a formvar film and observed with Libra 120 Plus transmission electron microscope.

3. Results

3.1. Spectroscopic studies of peptide folding and binding

The membrane activity of native magainin 2 is characterised by a structural transition from a predominantly unstructured state, to a predominantly α-helical structure [30], making far-UV CD a convenient method for comparing the propensity of the peptide to bind to different DPPG/DP3adLPG mixtures (Fig. 2A). At 25 °C, an excess of 60 and 70 mol% DPPG in the lipid mixtures elicited high degrees of α-helix formation by magainin 2 F5W (Table 1), although it is apparent that as the two lipids approached nearly equimolar proportions (DPPG/DP3adLPG [55:45]), the helical content diminished markedly. Increasing the DP3adLPG content above 50 mol% had little further effect on the α-helix content. In a parallel study of peptide binding to the lipid dispersions, using the fluorescence emission of the tryptophan residue as a reporter (Fig. 2B), the reduction in helical content of the peptide coincides with a reduction in detectable binding to the lipids (Table 2).

These results are similar to those we have previously reported for magainin 2 F5W interactions with DP3adLPG-containing vesicles at 55 °C (pH 7.4), where higher DPPG content resulted in high amounts of α-helix, which are reduced almost to zero in near equimolar anionic/

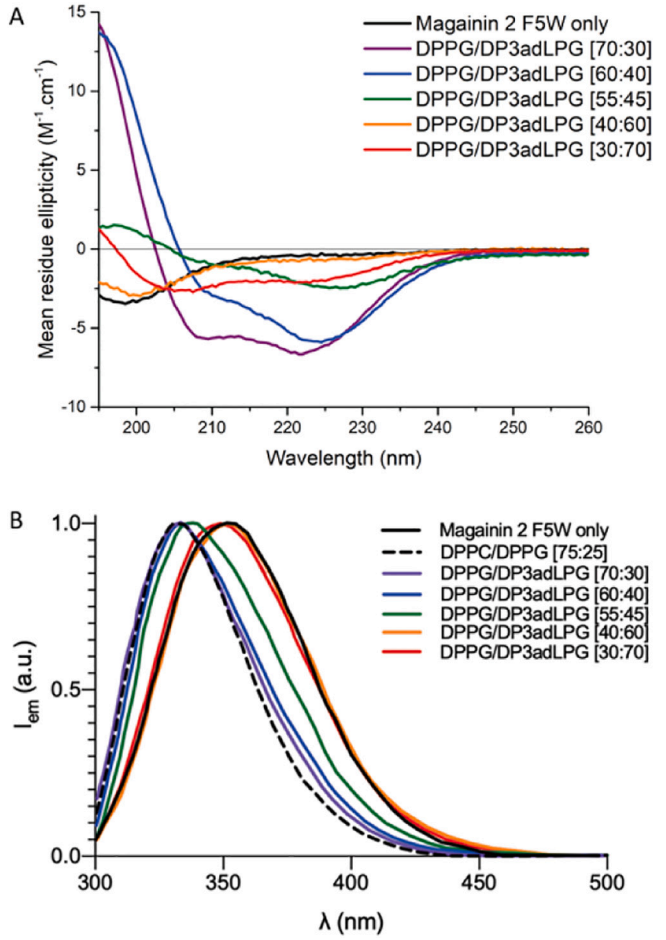

Fig. 2. (A) Static far-UV circular dichroism spectra and (B) normalised tryptophan fluorescence emission spectra (λ_{ex} 280 nm), for magainin 2 F5W in 70 mM Tris HCl buffer at pH 7.4, and in the presence of various lipid mixture dispersions at 25 °C.

Table 1
Calculated secondary structure content for magainin 2 F5W in 70 mM Tris HCl buffer (pH 7.4) and in the presence of various DPPG/DP3adLPG dispersions at 25 °C, obtained using the PLSPlus/IQ routine on GRAMS32 AI software (Galactic, USA) [19].

Sample	% a-helix	% b-sheet	% Other
Magainin 2 F5W	0.0	38.0	62.0
DPPG/DP3adLPG [70:30]	59.8	16.4	23.8
DPPG/DP3adLPG [60:40]	50.0	0.00	50.0
DPPG/DP3adLPG [55:45]	19.5	8.8	71.7
DPPG/DP3adLPG [40:60]	17.9	48.3	33.8
DPPG/DP3adLPG [30:70]	14.6	31.2	54.2

Table 2
Relative binding of magainin 2 F5W to vesicles with different lipid compositions calculated from normalised tryptophan emission spectra by comparing fluorescence intensities at 320 nm, assuming that DPPC/DPPG [75:25] vesicles elicit 100% binding.

Sample	λ_{max} (nm)	I_{320}	Relative binding %
Magainin 2 F5W	352.5	0.42	0
DPPC/DPPG [75:25]	331.8	0.82	100
DPPG/DP3adLPG [70:30]	334.5	0.82	100
DPPG/DP3adLPG [60:40]	332.9	0.79	88
DPPG/DP3adLPG [55:45]	338.4	0.70	70
DPPG/DP3adLPG [40:60]	350.3	0.42	0
DPPG/DP3adLPG [30:70]	348.3	0.47	12.5

cationic lipid mixtures [16].

3.2. Differential scanning calorimetry

The effects of thermal cycling on the two DPPG/DP3adLPG mixtures used in the neutron diffraction experiments were investigated by DSC (Fig. 3A) in order to confirm that the diffraction measurements were not performed within a phase transition. The thermal cycling of the DSC experiments mimicked the cycling procedure of the diffraction experiments. As solvent, 100 mM NaCl was used, because the ionic strength is necessary for vesicle formation and reproducible DSC curves with pure DPPG [31,32]. The individual lipids themselves exhibit similar thermotropic behaviours, where both were found to undergo their main gel to fluid phase transition (T_m) at ~41 °C (Fig. 3B). These are in agreement with previously reported T_m values for both DPPG [33] and lysyl-DPPG [12], measured at pH 7.4. The $L_{\beta'}$ to $P_{\beta'}$ pretransition for DPPG evident at 34 °C, is again consistent with literature values [33]. For DP3adLPG, however, the pretransition is absent, contrary to previous reports for its analogue lysyl-DPPG (38 °C) [12]. The structural difference or the ion content of the dispersant can explain this divergence.

The main transitions of both pure lipids are comparable: DPPG – T_m = 40.7 °C, FWHM = 0.96 °C, ΔH = 36.6 kJ/mol; DP3adLPG – T_m = 40.9 °C, FWHM = 0.48 °C, ΔH = 40.9 kJ/mol. The cooperativity of the

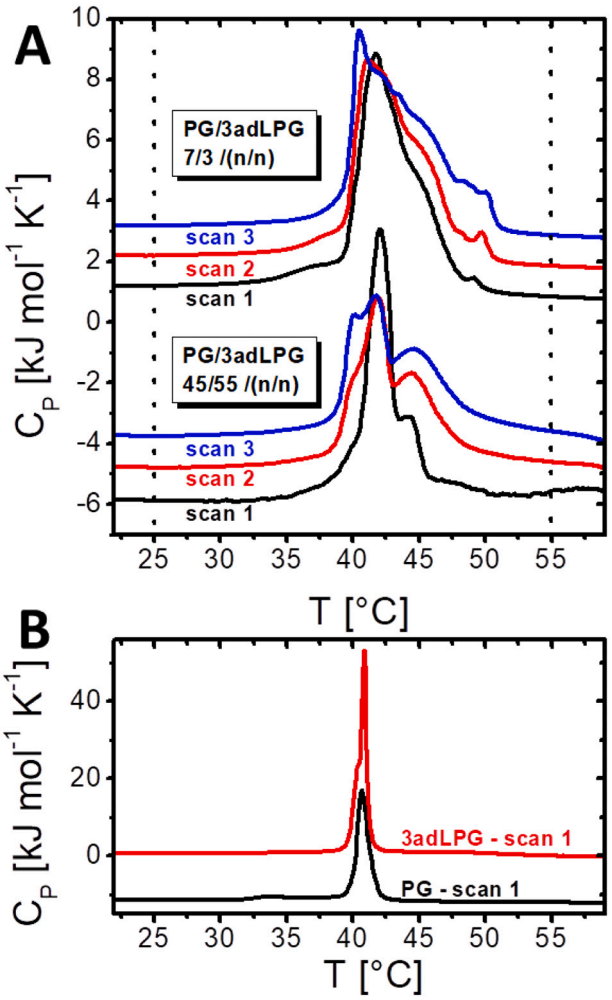

Fig. 3. DSC heating scans showing (A) the effect of temperature cycling on the main phase transitions of different DPPG/DP3adLPG mixtures in 100 mM NaCl (the dotted lines indicate the temperatures at which neutron diffraction experiments were conducted), and (B) the thermotropic phase transitions of pure DPPG and DP3adLPG. The curves are offset vertically for clarity.

transition is higher for the lysylated lipid, as indicated by the lower FWHM. Additional interactions in the head group of the lipid, possibly via H-bond network formation due to the carbonyl and amine moieties in the lysine, can explain this behaviour. The theory is also supported by the higher transition enthalpy observed for DP3adLPG. This can be explained by additional interactions in the head group which have to be overcome, as well as the van der Waals interactions between the alkyl chains, during the gel/fluid transition [34–37].

The DSC curves of both evaluated DPPG/DP3adLPG mixtures, show that no ideal miscibility of both lipids can be concluded, due to the multiple peaks. Additionally, there is a pronounced stabilisation of the gel phase in both mixtures. For the 45:55 mixture this effect can be seen due to a shoulder at around 45 °C. The formation of ion pairs between the lipids seems the most likely explanation for this behaviour [38]. The 70:30 mixture shows additional peaks at temperatures up to 50 °C, hence, the stabilisation of the gel phase is more pronounced. Previous work indicates that the formation of ion-triplets could explain this thermotropic behaviour [39].

The cycling experiments (scans 1–3) demonstrate that the neutron scattering experiments of the following sections were performed both below and above the phase transition (see the area indicated by the dashed lines in Fig. 3A).

3.3. Neutron diffraction

The neutron diffraction profile of the d_{62}DPPG/d_{62}DP3adLPG 70:30 mixture at 25 °C (Fig. 4A) shows that demixing effects occur in the gel phase, as indicated by the presence of two distinct lamellar phases, with d-spacing periodicities of 82 Å ($L_{\beta'}$ 1) and 62 Å ($L_{\beta'}$ 2) (Table 3). Two additional Bragg reflections at $q = 0.18$ Å^{-1} and $q = 0.28$ Å^{-1} (Fig. 4A - highlighted in green), could not be indexed as belonging to either $L_{\beta'}$ 1 or $L_{\beta'}$ 2, but may represent the second and third order reflections from an intermediate lamellar phase (with a theoretical d-spacing of 70.5 Å), the first order peak of which is masked by the more intense flanking peaks. The bilayer thicknesses of $L_{\beta'}$ 1 and $L_{\beta'}$ 2, as estimated from their SLD profiles (Fig. 6), were 48 Å (area per molecule 47.9 Å^2) and 42 Å (APM 54.7 Å^2) respectively (Table 3). The 20 Å difference in d-spacing between the two lamellar phases is therefore almost entirely due to a larger separation distance in $L_{\beta'}$ 1, probably facilitated by either electrostatic or steric repulsion forces. For instance, the presence of a separated PG-rich phase with a net negative charge can be assumed to result in $L_{\beta'}$ 1, while the $L_{\beta'}$ 2 could be dominated by PG/LPG ion pairs with a net charge of zero. Demixing effects diminish in the fluid phase, since increasing the temperature to 55 °C (Fig. 4C) results in the formation of a single fluid (L_α) lamellar phase with a d-spacing of 52 Å (Table 3) and a thinner (36.4 Å), more expanded (APM 63.1 Å^2) bilayer typical for acyl chain melting. The temperature dependent mixing/demixing behaviour is reversible with a distinct kinetic hinderance. Both the two distinct gel phases and the apparent intermediate phase remained present during temperature cycling (see Supporting information Fig. S6), although with decreased relative intensities for the $L_{\beta'}$ 1 Bragg reflections. Both the recognisable $L_{\beta'}$ and L_α phases were stable over the three heating/

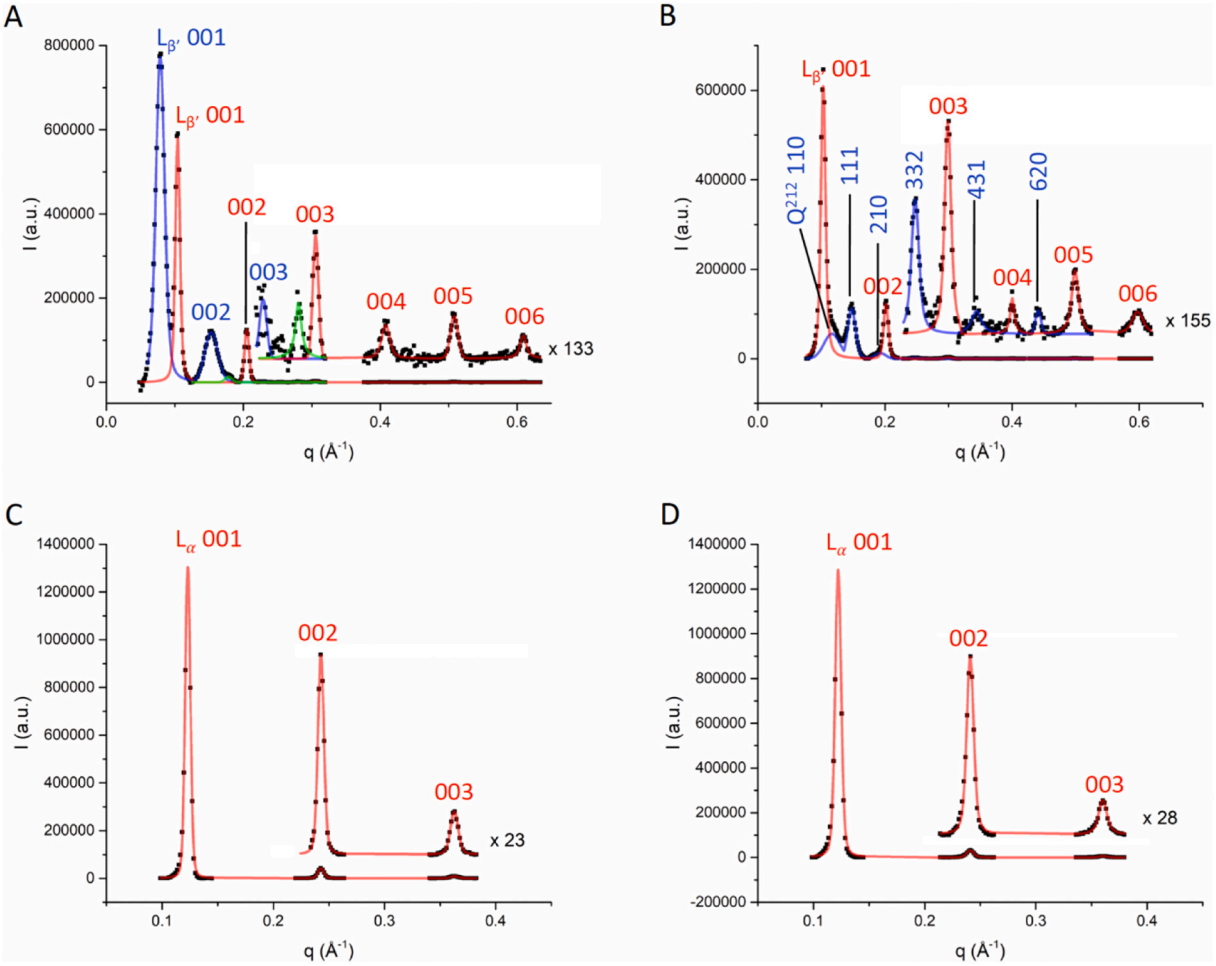

Fig. 4. Baseline-subtracted neutron diffraction patterns with Bragg peak indexing for d_{62}DPPG/d_{62}DP3adLPG 70:30 mixtures in H_2O, for lipids only at (A) 25 °C (the blue line shows $L_{\beta'}$ 1 and the red line shows $L_{\beta'}$ 2 associated Bragg Peaks) and (C) 55 °C and in the presence of 2 mol% magainin 2 F5W at (B) 25 °C (the red line shows $L_{\beta'}$ 2 related Bragg peaks) and (D) 55 °C. (For interpretation of the references to colour in this figure legend, the reader is referred to the web version of this article.)

Table 3
Lamellar phase parameters derived from neutron diffraction measurements performed on different d_{62}DPPG/d_{62}DP3adLPG mixtures in the presence and absence of 2 mol% magainin 2 F5W at either 25 °C or 55 °C.

Lipid mixture	Temp. (°C)	Phase	Peptide	d-spacing (Å)	Thickness (Å)	APM (Å^2)[a]
d_{62}DPPG/d_{62}DP3adLPG [70:30]	25	$L_{\beta'}$ 1	None	82	48	47.9
	25	$L_{\beta'}$ 1	Yes	n.d.	n.d.	n.d.
	25	$L_{\beta'}$ 2	None	62	42	54.7
	25	$L_{\beta'}$ 2	Yes	63	42	54.7
	55	L_a	None	52	36.4	63.1
	55	L_a	Yes	52	36	63.8
d_{62}DPPG/d_{62}DP3adLPG [55:45]	25	$L_{\beta'}$ 2	None	60	42	57.0
	25	$L_{\beta'}$ 2	Yes	62	44	54.4
	55	L_a	None	50	35	68.4
	55	L_a	Yes	51	34	70.4

n.d. not detected.
[a] Area per molecule (APM) estimated using the mean molecular volumes for each lipid mixture (see Supporting information Table S1).

cooling cycles undertaken during the neutron diffraction measurements.

The addition of 2 mol% magainin 2 F5W to the d_{62}DPPG/d_{62}DP3adLPG 70:30 lipid mixture, also resulted in the formation of two distinct phases at 25 °C (Fig. 4B). The $L_{\beta'}$ 2 phase appears to be little affected by the presence of the peptide, showing no detectable change in layer thickness or molecular area (Table 3). Comparing the SLD profiles of the $L_{\beta'}$ 2 phase with and without the peptide by subtracting one from the other (Fig. 7A), reveals only small differences in SLD in the head-group regions (deviation in the difference profile from zero), which may suggest some association of the peptide is occurring at the bilayer interface.

The most obvious effect of the peptide on the gel phase d_{62}DPPG/d_{62}DP3adLPG 70:30 mixture is the transformation of the $L_{\beta'}$ 1 phase to a non-lamellar phase which could be indexed as a $P4_332$ (Q^{212}) primitive cubic phase (see Supporting information Fig. S4) [28] with a lattice constant of 73 Å. This marked preference of the peptide to interact with the $L_{\beta'}$ 1 phase and not the $L_{\beta'}$ 2 phase, suggest that the former is rich in DPPG, thus attracting the cationic peptide via electrostatic interaction [30]. This thesis fits with the assumption made above, that the $L_{\beta'}$ 1 phase has a net negative charge due to the excess DPPG and therefore

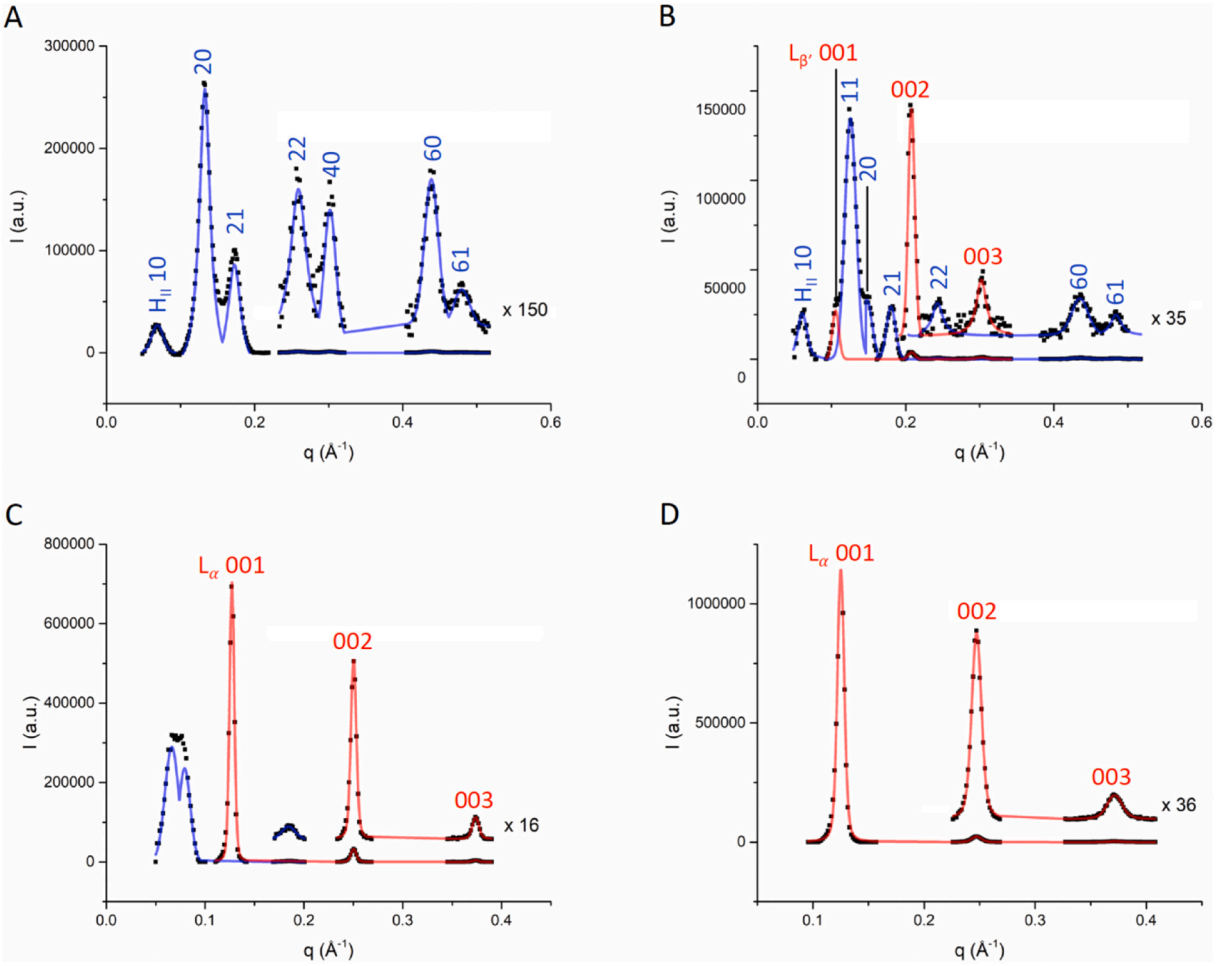

Fig. 5. Baseline-subtracted neutron diffraction patterns with Bragg peak indexing for d_{62}DPPG/d_{62}DP3adLPG 45:55 mixtures in H_2O, for lipids only at (A) 25 °C and (C) 55 °C (the blue line shows the presence of residual non-lamellar phase) and in the presence of 2 mol% magainin 2 F5W at (B) 25 °C (the red line shows $L_{\beta'}$ 2 related Bragg peaks) and (D) 55 °C. (For interpretation of the references to colour in this figure legend, the reader is referred to the web version of this article.)

the larger d-spacing is attributable to charge repulsion. Increasing the temperature to 55 °C results in the formation of a single L_α phase which shows only slight differences in the SLD profile from the peptide-free sample (Fig. 7B), in the headgroup region, suggesting binding rather than penetration of the peptide into the bilayer [16].

In the case of the d_{62}DPPG/d_{62}DP3adLPG 45:55 mixture at 25 °C (Fig. 5A), the first diffraction measurement in the H_2O contrast presented as consisting of only non-lamellar phase, which could be indexed as an inverse hexagonal (H_{II}) phase (see Supporting information Fig. S5A) with a lattice constant of 100 Å. After heating to 55 °C and recooling to 25 °C to measure diffraction in additional contrasts, the $L_{\beta'}$ 2 phase (Table 3) was detected again, mixed with an H_{II} phase (see Supporting information Figs. S5B and S7A), with a lattice constant of 96 Å. There seems to be a kinetic hindrance of the formation of the lamellar phase after hydration of the lipid with solvent vapour.

Above 55 °C there remains some non-lamellar phase (non-indexable) on the first heating cycle, mixed with the L_α phase, which becomes the only detectable content after additional temperature cycling (see Supporting information Fig. S7C). Although the d-spacing and bilayer thickness of the L_α phase were both similar to those determined for the d_{62}DPPG/d_{62}DP3adLPG 70:30 mixture (~50 Å and 35 Å respectively), the average molecular area was calculated to be 68.4 $Å^2$, being slightly larger for the 45:55 mixture (Table 3).

Addition of magainin 2 F5W to the d_{62}DPPG/d_{62}DP3adLPG 45:55 mixture at 25 °C does not induce the formation of any indexable cubic phase, as was observed for the 70:30 mixture, but remains a mixture of the H_{II} (lattice constant = 100 Å) and $L_{\beta'}$ 2 phases, a coexistence which is stable during temperature cycling (Fig. 5B, Supporting information Fig. S7B). The fact that the repeat spacing of the H_{II} remains unchanged in the presence of the magainin 2 F5W, suggests that there is little or no interaction of the peptide with this phase.

Although comparisons between the SLD profiles of the $L_{\beta'}$ 2 phases in the presence and absence of magainin 2 F5W are made problematic due to differences in the patterns of lamellar phase Bragg reflections observed for the two samples, Fig. 5C indicates that in keeping with the observation made for the 70:30 mixture, the peptide appears to associate with the headgroup region of the bilayers.

Increasing the temperature to 55 °C resulted in the formation of a single L_α phase (Fig. 5D) which remained stable after temperature cycling (see Supporting information Fig. S7D). Compared to the peptide-free 45:55 mixture, the L_α phase in the presence of magainin 2 F5W showed a slight thinning of the bilayer and increase in mean molecular area (Table 3), which may be attributable to peptide interaction, again, apparently localised to the interfacial region of the bilayers (Fig. 7D).

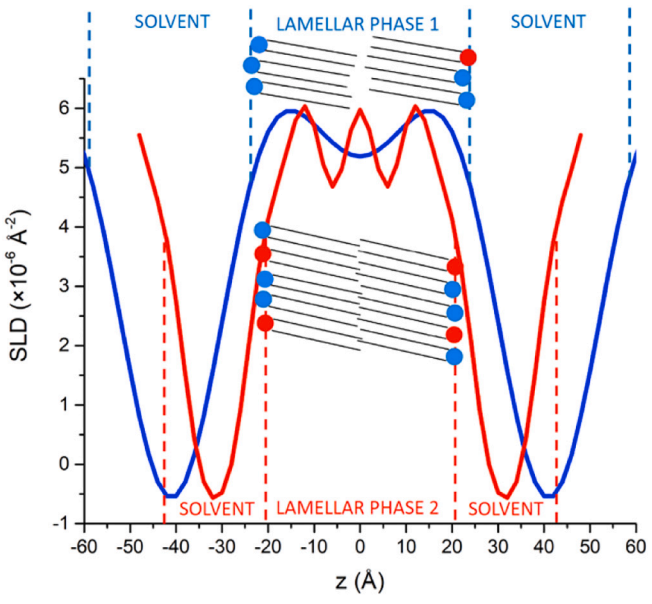

Fig. 6. Normalised neutron scattering length density (SLD) profiles for the two lamellar phases detected in the d_{62}DPPG/d_{62}DP3adLPG 70:30 mixture in H_2O at 25 °C: $L_{\beta'}$ Phase 1 (blue profile) and $L_{\beta'}$ Phase 2 (red profile). The cartoons show the putative distribution of the lipids between the two phases, where the blue headgroup represents d_{62}DPPG and red represents the d_{62}DP3adLPG. (For interpretation of the references to colour in this figure legend, the reader is referred to the web version of this article.)

3.4. Cryo-transmission electron microscopy

Evidence for the formation of non-lamellar phases in DPPG/DP3adLPG mixtures, was also obtained from samples prepared for electron microscopy. Although the lipid mixtures created for cryo-TEM studies were dispersed in a large excess of water using a small input of energy, provided by an ultrasonic bath, and were thus in marked contrast to the passive formation of the vapour-solvated bilayer stacks created for the neutron diffraction measurements, differences in morphologies between the two lipid mixtures were clearly discernible (Fig. 8). Even after the limited use of bath sonication, the DPPG/DP3adLPG 70:30 mixture consisted mainly of size-polydisperse large unilamellar vesicles with noticeably irregularly polyhedral morphologies (Fig. 8A). Although the presence of these vesicles does not preclude the possibility that they consisted of mixed lamellar phase domains as evidenced by the diffraction studies, these were not apparent from the electron micrographs. In contrast, there are a number of aggregate morphologies apparent in the sample prepared from the DPPG/DP3adLPG 45:55 mixture (Fig. 8B). Although some large unilamellar vesicles were visible, there were many more highly lipid rich structures visible, which were rapidly damaged by the microscope's electron beam. These lipid rich structures appear to be very similar to those previously described as possessing large numbers of inter-lamellar attachments (ILA), which are intermediates between lamellar and reverse hexagonal phases [40]. Interspersed within the samples were aggregates which were more readily identifiable as fragments of H_{II} phase (Fig. 8B insert) [41].

3.5. Freeze-fracture electron microscopy

The freeze-fracture electron micrographs taken of the DPPG/DP3adLPG 70:30 mixture, show a mixture of small and large, predominantly unilamellar, vesicles (Fig. 9A). Magnified images of single vesicles whose fracture plane was likely to be within the bilayer, rather than bisecting whole vesicles, reveal in more detail the irregular polyhedral patchwork of the vesicle surfaces (Fig. 9B).

Although the images taken from the DPPG/DP3adLPG 45:55 mixture dispersion (Fig. 9C & D) do not show any structures which were readily identifiable as inverse hexagonal phases, they did contain mixtures of vesicular structures and more dense lipid-rich regions which lack a discrete multi-lamellar structure, but instead resemble more flexible highly-curved structures which may have the propensity to facilitate fusion between adjacent bilayers [42]. Such structures are similar to the ILA observed in the cryo-TEM samples, and may be indicative of lamellar to reverse hexagonal phase intermediates [41].

4. Discussion

It is clear from the results presented in this study, that the phase behaviour of DPPG/DP3adLPG mixtures is quite complex and is dependent on a number of factors, including the relative proportions of the lipids, their physical state (with solid or melted acyl chains), the ability of their headgroups to form ionic associations (itself dependent upon the degree of ionisation of the 3adLPG headgroup) and the degree of system hydration. In the neutron diffraction profiles of the gel phase peptide-free samples, two distinct phases were observed in each of the mixtures (70:30 and 55:45), with only the ~62 Å periodicity $L_{\beta'}$ 2 phase

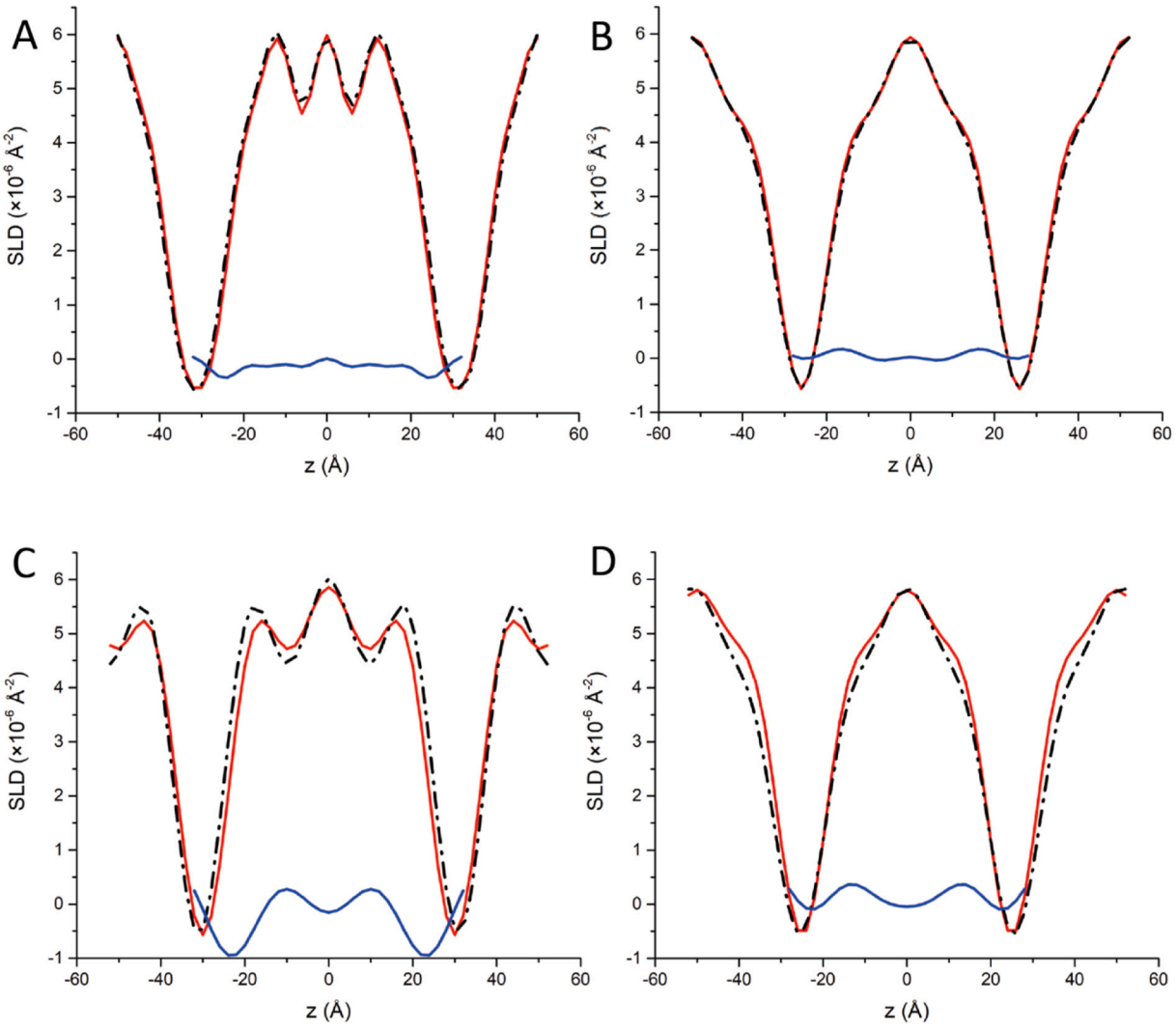

Fig. 7. Normalised neutron SLD profiles of lipids alone (solid red lines) and lipids in the presence of 2 mol% magainin 2 F5W (dashed black line), together with their difference profiles (solid blue line) for (A) d_{62}DPPG/d_{62}DP3adLPG 70:30 mixture $L_{\beta'}$ Phase 2 at 25 °C, (B) d_{62}DPPG/d_{62}DP3adLPG 70:30 mixture L_{α} phase at 55 °C, (C) d_{62}DPPG/d_{62}DP3adLPG 45:55 mixture $L_{\beta'}$ phase at 25 °C and (D) d_{62}DPPG/d_{62}DP3adLPG 45:55 mixture L_{α} phase at 55 °C. All of the unit cell SLD profiles were constructed using Eq. (3) by assigning the H_2O contrast Bragg peak phases + − + + + +. The blue line is the residual after subtracting the profile in the presence of magainin 2 F5W from the one without peptide. (For interpretation of the references to colour in this figure legend, the reader is referred to the web version of this article.)

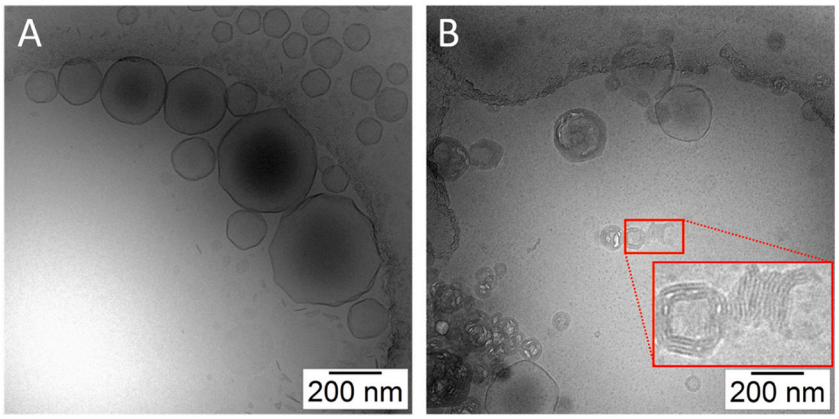

Fig. 8. Cryo-transmission electron micrographs of (A) DPPG/DP3adLPG 70:30 mixture, and (B) DPPG/DP3adLPG 45:55 mixture, prepared from dispersions in water at 25 °C.

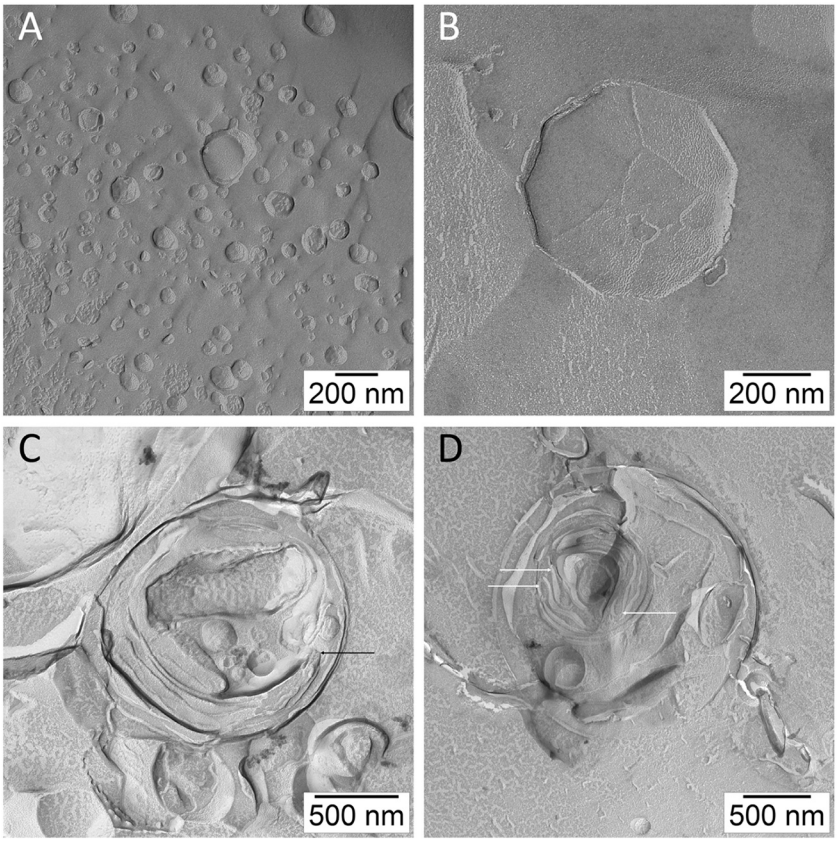

Fig. 9. Freeze fracture electron micrographs of (A, B) DPPG/DP3adLPG 70:30 mixture, and (C, D) DPPG/DP3adLPG 45:55 mixture, prepared from dispersions in water at 25 °C. Arrows indicate regions of high membrane curvature.

being common to both. In the fluid phase samples, the diffraction profiles for both mixtures show the presence of a ~51 Å periodicity L_{α} phase, suggesting ideal mixing of the lipid species above the melting transition regardless of lipid composition. It is the reproducible phase separation, occurring upon the cooling cycle, which points to a genuine demixing phenomenon in the gel phase. Since both pure DPPG and DP3adLPG undergo chain melting transitions at ~41 °C, but exhibit significantly different thermotropic behaviours with multiple transitions when mixed, the demixing behaviour must be driven by a variety of different interactions occurring between the headgroups of the two lipids.

As the samples prepared for the neutron diffraction measurements were solvated by water or D_2O vapour, the pH of the solvent layers would be determined by the concentrations of the two lipid counter ions, triethylammonium (d_{62}DPPG) and trifluoroacetate (d_{62}DP3adLPG). For the d_{62}DPPG/d_{62}DP3adLPG 70:30 mixture, the excess of trimethylammonium would most likely create a weakly acidic headgroup solvent environment, which would favour the full ionisation of the d_{62}DP3adLPG, and thus facilitate ion pairing between the two oppositely-charged lipids [6]. Even in the absence of any zwitterionic d_{62}DP3adLPG, ion pairing would only sequester a maximum of 43% of the d_{62}DPPG molecules present. The excess of unpaired d_{62}DPPG could form a separate phase from the d_{62}DPPG-d_{62}DP3adLPG ion pairs, resulting in the two predominant lamellar phases observed by neutron diffraction at 25 °C. The distinctive d-spacing periodicities of these two phases (with evidence of only a small quantity of a third hybrid periodicity phase), indicates that for the most part they possess long range order in the form of phase-separated bilayer stacks with symmetric or coupled leaflets [43,44]. The larger d-spacing of the $L_{\beta'}$ 1 phase (82 Å), suggests that this is the d_{62}DPPG-rich phase, which would be expected to possess a larger periodicity due to electrostatic repulsion between the like-charged stacked bilayers [45], and a slightly thicker bilayer due to a reduced chain tilt angle compared to mixtures with higher DP3adLPG content [6]. Using the AMP magainin 2 F5W as a probe provides further evidence for the identification of the $L_{\beta'}$ 1 phase, as co-deposition of the lipids with the peptide results in the loss of the $L_{\beta'}$ 1 phase and the concomitant appearance of a non-lamellar phase which could be indexed as a $P4_332$ (Q^{212}) primitive cubic phase. Induction of non-lamellar or specific cubic phase structures have been observed in other synthetic bacterial membrane models upon interaction with various AMPs [46,47]. The CD data shows that magainin 2 F5W favours interaction with gel phase mixed bilayers containing over 40% DPPG, and since native magainin 2 is known to interact preferentially with anionic lipids [30], this finding also suggests that $L_{\beta'}$ 1 is PG-rich. This implies that the $L_{\beta'}$ 2 phase may predominantly consist of d_{62}DPPG-d_{62}DP3adLPG ion pairs since its charge neutrality [6], would discourage interaction with the peptide. However, examining the neutron diffraction results from the d_{62}DPPG/d_{62}DP3adLPG 45:55 mixture suggests that the in reality the phase compositions may be more complicated.

Assuming again that a weakly acidic headgroup environment of the d_{62}DPPG/d_{62}DP3adLPG 45:55 mixture, would favour full ionisation of d_{62}DP3adLPG and thus ion pair formation, the d_{62}DPPG-d_{62}DP3adLPG complex would be expected to be the most common constituent present. The initial diffraction measurement at 25 °C, however, shows no evidence of a stacked $L_{\beta'}$ 2 phase, which only appears after the first heating/cooling cycle. The predominance of the H_{II} phase below the melting phase transition temperature, would seem to imply that this is most likely formed exclusively by d_{62}DPPG-d_{62}DP3adLPG ion pairs. Indeed, the formation of reverse hexagonal phases by equimolar mixtures of bilayer-forming cationic and anionic lipids, has been observed previously in fully-solvated bulk systems containing dioleoylethylphosphocholine (EDOPC) and beef heart cardiolipin [48]. The formation of a d_{62}DPPG-d_{62}DP3adLPG neutral ion pair, which excludes counter ions from the interfacial region and possesses a reduced

molecular area compared to the unpaired lipids [6], would be expected to also exhibit a reduced headgroup hydration [38,49]. The reduction in the size of the headgroup hydration shell, compounded by the loss of counter ions, increases the tendency of the lipid ion pairs to adopt a packing geometry with increased negative curvature, thus resulting the formation of an inverted hexagonal phase [50,51]. The propensity for d_{62}DPPG-d_{62}DP3adLPG ion pairs to form an H_{II} phase may be aided by the reduced solvent content of the vapour-hydrated samples used for the neutron diffraction studies. In bulk systems with excess water, such as those examined using a combination of cryo-transmission and freeze fracture electron microscopy, the DPPG/DP3adLPG 45:55 mixture appears to form a mixture of lamellar phase and inverse hexagonal or highly flexible intermediate structures. Some stacked lamellar phase was also detected at 25 °C by neutron diffraction after heating and recooling, which exhibited strikingly similar d-spacing, thickness and molecular area to the $L_{\beta'}$ 2 phase observed in the 70:30 mixture.

The thermotropic behaviour of the two mixtures provides some evidence which could aid the identification of the $L_{\beta'}$ 2 phase. The increased stabilisation of the gel phase observed in the thermograms for the DPPG/DP3adLPG 70:30 mixture, is similar to that which was previously reported for an anionic lipid/cationic surfactant 2:1 mixture, which we attributed to the formation of putative ion triplet complexes [38]. With sufficient localised excess of PG, ion pairing with adjacent 3adLPG may continually switch between different PG molecules, resulting in a type of resonance structure in which the overall anionic charge is diffused over the three constituent lipid headgroups. The formation of DPPG-DP3adLPG-DPPG complexes may thus be favoured over that of the other phases, due simply to local proportions of the lipids, and then demix from either the DPPG-rich phase or the DPPG-DP3adLPG ion pairs, on the basis of their different chain packing geometries [6]. The more diffuse anionic charge of these complexes, would not be as attractive to the magainin 2 F5W peptide probe, when in the presence of the PG-rich phase, but may nevertheless be strong enough to bind the peptide at the interfacial region without allowing deeper penetration into the chains [13,16] when in the presence of the non-attracting ion paired phase. Upon heating, the melting of the acyl chains disrupts the different chain lattices and allows full miscibility of the lipids, and the formation of a more homogeneous L_{α} phase. Even in the fluid phase, however, associations between DPPG and DP3adLPG, have been shown to influence membrane ordering and thus probably survive as discrete molecular complexes despite the change in state [16].

The relevance of the PG/3adLPG mixture polymorphism observed in the simple *S. aureus* membrane model presented in this study, to the behaviour of native L-PG in complex bacterial membranes, needs to be established through further research. The widely-observed heterogeneity of bacterial membranes is mediated through a combination of lipid-lipid, protein-protein and lipid-protein interactions [52], which facilitate the structuring of the membrane into functional domains whose differing lipid composition may be altered at different periods of the cell cycle [53,54], or in response to environmental stress [55]. Although the spatial organisation of membrane regions rich in anionic lipids such as cardiolipin (at cell poles) and phosphatidylglycerol (helical domains along the cell) are well characterised for *Bacillus subtilis* [56], less is known about the presence of such domains in *S. aureus*, beyond the existence of PG-rich regions at the cell septum during binary fission [57]. With respect to investigations into the possible physiological functions of lysyl-PG in *S. aureus*, these have mainly centred on its role in resistance to cationic antimicrobial peptides [58], and as a putative suppressor of DNA replication initiation, through inhibition of CL and PG-mediated ATP release from DnaA protein [59]. It might be argued that both of these processes could be primarily driven by the membrane charge neutralisation facilitated by increased LPG biosynthesis in *S. aureus* [10]. However, as has been demonstrated through the use of our 3adLPG substitute, the presence of LPG could play a much wider role in membrane structuring and lateral organisation in *S. aureus*, through its varied associations with PG, and the different ways in which lipid ion pairs or triplets influence membrane behaviour. Indeed the propensity for DPPG-DP3adLPG ion pairs to form inverse hexagonal phases, may provide an alternative explanation for their role in AMP resistance aside from their charge neutrality, since it has long been demonstrated that the presence of neutral lipids which impart negative curvature to bacterial membranes also inhibit AMP activity [60].

Declaration of competing interest

The authors declare that they have no known competing financial interests or personal relationships that could have appeared to influence the work reported in this paper.

Acknowledgements

The authors wish to thank the Institut Laue-Langevin for the allocation of beam-time (experiment number 8-02-618) and use of laboratory preparation facilities within the Partnership for Soft Condensed Matter. RR was financially supported by a studentship from the Biotechnology and Biological Sciences Research Council (UK). RDH was financially supported by a Next Generation Facility Users Grant (EP/G068569/1) from the Engineering and Physical Sciences Research Council (UK).

Appendix A. Supplementary data

Supplementary data to this article can be found online at https://doi.org/10.1016/j.bbamem.2021.183571.

References

[1] M. Li, D.J. Cha, Y. Lai, A.E. Villaruz, D.E. Sturdevant, M. Otto, The antimicrobial peptide-sensing system aps of Staphylococcus aureus, Mol. Microbiol. 66 (2007) 1136–1147, https://doi.org/10.1111/j.1365-2958.2007.05986.x.

[2] C.M. Ernst, C.J. Slavetinsky, S. Kuhn, J.N. Hauser, M. Nega, N.N. Mishra, C. Gekeler, A.S. Bayer, A. Peschel, Gain-of-function mutations in the phospholipid flippase MprF confer specific daptomycin resistance, MBio. 9 (2018), e01659-18, https://doi.org/10.1128/mBio.01659-18.

[3] T. Jones, M.R. Yeaman, G. Sakoulas, S.-J. Yang, R.A. Proctor, H.-G. Sahl, J. Schrenzel, Y.Q. Xiong, A.S. Bayer, Failures in clinical treatment of Staphylococcus aureus infection with daptomycin are associated with alterations in surface charge, membrane phospholipid asymmetry, and drug binding, Antimicrob. Agents Chemother. 52 (2008) 269–278, https://doi.org/10.1128/AAC.00719-07.

[4] C.M. Ernst, A. Peschel, Broad-spectrum antimicrobial peptide resistance by MprF-mediated aminoacylation and flipping of phospholipids, Mol. Microbiol. 80 (2011) 290–299, https://doi.org/10.1111/j.1365-2958.2011.07576.x.

[5] J.F. Tocanne, P.H.J. Ververgaert, A.J. Verkleij, L.L.M. Van Deenen, A monolayer and freeze-etching study of charged phospholipids II. Ionic properties of mixtures of phosphatidylglycerol and lysylphosphatidylglycerol, Chem. Phys. Lipids. 12 (1974) 220–231.

[6] C. Wölk, H. Youssef, T. Guttenberg, H. Marbach, G. Vizcay-Barrena, C. Shen, G. Brezesinski, R.D. Harvey, Phase diagram for a lysyl-phosphatidylglycerol analogue in biomimetic mixed monolayers with phosphatidylglycerol: insights into the tunable properties of bacterial membranes, ChemPhysChem. (2020) cphc.202000026. doi:https://doi.org/10.1002/cphc.202000026.

[7] K. Mukhopadhyay, W. Whitmire, Y.Q. Xiong, J. Molden, T. Jones, A. Peschel, P. Staubitz, J. Adler-Moore, P.J. McNamara, R.A. Proctor, M.R. Yeaman, A. S. Bayer, In vitro susceptibility of Staphylococcus aureus to thrombin-induced platelet microbicidal protein-1 (tPMP-1) is influenced by cell membrane phospholipid composition and asymmetry, Microbiology-Sgm. 153 (2007) 1187–1197, https://doi.org/10.1099/mic.0. 2006/003111-0.

[8] A.S. Bayer, N.N. Mishra, L. Chen, B.N. Kreiswirth, A. Rubio, S.J. Yang, Frequency and distribution of single-nucleotide polymorphisms within mprF in methicillin-resistant Staphylococcus aureus clinical isolates and their role in cross-resistance to daptomycin and host defense antimicrobial peptides, Antimicrob. Agents Chemother. 59 (2015) 4930–4937, https://doi.org/10.1128/AAC.00970-15.

[9] C.M. Ernst, P. Staubitz, N.N. Mishra, S.-J. Yang, G. Hornig, H. Kalbacher, A. S. Bayer, D. Kraus, A. Peschel, The bacterial defensin resistance protein MprF consists of separable domains for lipid lysinylation and antimicrobial peptide repulsion, PLoS Pathog. 5 (2009), e1000660, https://doi.org/10.1371/journal.ppat.1000660.

[10] R.P. Rehal, H. Marbach, A.T.M. Hubbard, A.A. Sacranie, F. Sebastiani, G. Fragneto, R.D. Harvey, The influence of mild acidity on lysyl-phosphatidylglycerol biosynthesis and lipid membrane physico-chemical properties in methicillin-resistant Staphylococcus aureus, Chem. Phys. Lipids 206 (2017) 60–70, https://doi.org/10.1016/j.chemphyslip.2017.06.007.

[11] E. Kilelee, A. Pokorny, M.R. Yeaman, A.S. Bayer, Lysyl-phosphatidylglycerol attenuates membrane perturbation rather than surface association of the cationic antimicrobial peptide 6W-RP-1 in a model membrane system: implications for daptomycin resistance, Antimicrob. Agents Chemother. 54 (2010) 4476–4479, https://doi.org/10.1128/AAC.00191-10.

[12] S. Danner, G. Pabst, K. Lohner, A. Hickel, Structure and thermotropic behavior of the Staphylococcus aureus lipid lysyl-dipalmitoylphosphatidylglycerol, Biophys. J. 94 (2008) 2150–2159, https://doi.org/10.1529/biophysj.107.123422.

[13] E. Cox, A. Michalak, S. Pagentine, P. Seaton, A. Pokorny, Lysylated phospholipids stabilize models of bacterial lipid bilayers and protect against antimicrobial peptides, Biochim. Biophys. Acta (BBA)-Biomembranes. 1838 (2014) 2198–2204.

[14] S.H. Collins, W.A. Hamilton, Magnitude of the protonmotive force in respiring Staphylococcus aureus and Escherichia coli, J. Bacteriol. 126 (1976) 1224–1231.

[15] J.F. Tocanne, P.H.J.T. Ververgaert, A.J. Verkleij, L.L.M. van Deenen, A monolayer and freeze-etching study of charged phospholipids I. Effects of ions and pH on the ionic properties of phosphatidylglycerol and lysylphosphatidylglycerol, Chem. Phys. Lipids. 12 (1974) 201–219. doi:https://doi.org/10.1016/0009-3084(74)90075-9.

[16] R. Rehal, P.R.J. Gaffney, A.T.M. Hubbard, R.D. Barker, R.D. Harvey, The pH-dependence of lipid-mediated antimicrobial peptide resistance in a model staphylococcal plasma membrane: a two-for-one mechanism of epithelial defence circumvention, Eur. J. Pharm. Sci. 128 (2019) 43–53, https://doi.org/10.1016/j.ejps.2018.11.017.

[17] H. Marbach, G. Vizcay-Barrena, K. Memarzadeh, J.A. Otter, S. Pathak, R.P. Allaker, R.D. Harvey, J.D. Edgeworth, Tolerance of MRSA ST239-TW to chlorhexidine-based decolonization: evidence for keratinocyte invasion as a mechanism of biocide evasion, J. Inf. Secur. 78 (2019) 119–126, https://doi.org/10.1016/j.jinf.2018.10.007.

[18] R. Rehal, A Physicochemical and Biophysical Investigation Into the Role of Lysyl-phosphatidylglycerol in the Membrane of *Staphylococcus aureus* Under Mild Acidic Conditions., King's College London, 2014.

[19] K.M. Malik, Chemometric and Quantum Mechanical Methods for Analysing CD Spectra., University of London, 1997. https://scholar.google.de/scholar?hl=en&as_sdt=0%2C5&authuser=1&q=Chemometric+and+Quantum+Mechanical+Methods+for+Analysing+CD+spectra&btnG= (accessed June 2, 2020).

[20] A.S. Ladokhin, S. Jayasinghe, S.H. White, How to measure and analyze tryptophan fluorescence in membranes properly, and why bother? Anal. Biochem. 285 (2000) 235–245, https://doi.org/10.1006/abio.2000.4773.

[21] F. Sebastiani, R. Harvey, S. Khanniche, J.B. Artero, M. Haertlein, G. Fragneto, Diffraction studies on natural and model lipid bilayers, Eur. Phys. J. Spec. Top. 213 (2012) 355–365, https://doi.org/10.1140/epjst/e2012-01682-3.

[22] E.H. Mojumdar, D. Groen, G.S. Gooris, D.J. Barlow, M.J. Lawrence, B. Deme, J. A. Bouwstra, Localization of cholesterol and fatty acid in a model lipid membrane: a neutron diffraction approach, Biophys. J. 105 (2013) 911–918, https://doi.org/10.1016/j.bpj.2013.07.003.

[23] NIST, Center for Neutron Research, Neutron Diffraction Analysis of the Structure of a Phospholipid Bilayer Membrane With Deuterated Hydrocarbon Chains Using the Advanced Neutron Diffractometer/Reflectometer (AND/R), Gaithersburg, MD. https://www.ncnr.nist.gov/summerschool/ss06/WorcesterExperiment.pdf, 2006. (Accessed 9 June 2020).

[24] N.P. Franks, W.R. Lieb, The structure of lipid bilayers and the effects of general anaesthetics. An X-ray and neutron diffraction study, J. Mol. Biol. 133 (1979) 469–500. doi:https://doi.org/10.1016/0022-2836(79)90403-0.

[25] Neutron Activation and Scattering Calculator, (n.d.). https://www.ncnr.nist.gov/resources/activation/ (accessed April 12, 2019).

[26] J.F. Nagle, S. Tristram-Nagle, Structure of lipid bilayers, Biochim. Biophys. Acta - Rev. Biomembr. 1469 (2000) 159–195, https://doi.org/10.1016/S0304-4157(00)00016-2.

[27] J.M. Seddon, R.H. Templer, Polymorphism of lipid-water systems, in: R. Lipowsky, E. Sackmann (Eds.), Handb. Biol. Phys., Elsevier Science B.V., 1995: pp. 97–160. doi:https://doi.org/10.1016/S1383-8121(06)80020-5.

[28] R. Winter, R. Köhling, Static and time-resolved synchrotron small-angle x-ray scattering studies of lyotropic lipid mesophases, model biomembranes and proteins in solution, J. Phys. Condens. Matter. 16 (2004) S327–S352, https://doi.org/10.1088/0953-8984/16/5/002.

[29] J. Lendermann, R. Winter, Interaction of cytochrome c with cubic monoolein mesophases at limited hydration conditions: the effects of concentration, temperature and pressure, Phys. Chem. Chem. Phys. 5 (2003) 1440–1450, https://doi.org/10.1039/b209825n.

[30] K. Matsuzaki, Magainins as paradigm for the mode of action of pore forming polypeptides, Biochim. Biophys. Acta - Rev. Biomembr. 1376 (1998) 391–400, https://doi.org/10.1016/S0304-4157(98)00014-8.

[31] K.K. Eklund, I.S. Salonen, P.K.J. Kinnunen, Monovalent cation dependent phase behaviour of dipalmitoylphosphatidylglycerol, Chem. Phys. Lipids 50 (1989) 71–78, https://doi.org/10.1016/0009-3084(89)90028-5.

[32] G. Cevc, A. Watts, D. Marsh, Non-electrostatic contribution to the titration of the ordered-fluid phase transition of phosphatidylglycerol bilayers, FEBS Lett. 120 (1980) 267–270, https://doi.org/10.1016/0014-5793(80)80313-9.

[33] Y.P. Zhang, R.N.A.H. Lewis, R.N. McElhaney, Calorimetric and spectroscopic studies of the thermotropic phase behavior of the n-saturated 1,2-diacylphosphatidylglycerols, Biophys. J. 72 (1997) 779–793, https://doi.org/10.1016/S0006-3495(97)78712-5.

[34] G. Cevc, How membrane chain melting properties are regulated by the polar surface of the lipid bilayer, Biochemistry. 26 (1987) 6305–6310, https://doi.org/10.1021/bi00394a002.

[35] M.J. Blandamer, B. Briggs, P.M. Cullis, J.B.F.N. Engberts, R.I. Norman, Influence of polar head groups on the gel to liquid-crystal transition in vesicular and lipid bilayer systems, J. Chem. Soc. - Faraday Trans. 92 (1996) 3163–3164, https://doi.org/10.1039/ft9969203163.

[36] R.D. Koynova, H.L. Kuttenreich, B.G. Tenchov, H.J. Hinz, Influence of head-group interactions on the miscibility of synthetic, stereochemically pure glycolipids and phospholipids, Biochemistry. 27 (1988) 4612–4619, https://doi.org/10.1021/bi00413a005.

[37] A. Blume, A comparative study of the phase transitions of phospholipid bilayers and monolayers, BBA - Biomembr. 557 (1979) 32–44, https://doi.org/10.1016/0005-2736(79)90087-7.

[38] M. Schmid, C. Wölk, J. Giselbrecht, K.L.A. Chan, R.D. Harvey, A combined FTIR and DSC study on the bilayer-stabilising effect of electrostatic interactions in ion paired lipids, Colloids Surfaces B Biointerfaces. 169 (2018) 298–304, https://doi.org/10.1016/j.colsurfb.2018.05.031.

[39] C. Wölk, G. Hause, O. Gutowski, R.D. Harvey, G. Brezesinski, Enhanced chain packing achieved via putative headgroup ion-triplet formation in binary anionic lipid/cationic surfactant mixed monolayers, Chem. Phys. Lipids 225 (2019) 104827, https://doi.org/10.1016/J.CHEMPHYSLIP.2019.104827.

[40] D.P. Siegel, W.J. Green, Y. Talmon, The mechanism of lamellar-to-inverted hexagonal phase transitions: a study using temperature-jump cryo-electron microscopy, Biophys. J. 66 (1994) 402–414, https://doi.org/10.1016/S0006-3495(94)80790-8.

[41] D.P. Siegel, J.L. Burns, M.H. Chestnut, Y. Talmon, Intermediates in membrane fusion and bilayer/nonbilayer phase transitions imaged by time-resolved cryo-transmission electron microscopy, Biophys. J. 56 (1989) 161–169, https://doi.org/10.1016/S0006-3495(89)82661-X.

[42] V.L. Borovjagin, J.A. Vergara, T.J. McIntosh, Morphology of the intermediate stages in the lamellar to hexagonal lipid phase transition, J. Membr. Biol. 69 (1982) 199–212, https://doi.org/10.1007/BF01870399.

[43] L. Tayebi, Y. Ma, D. Vashaee, G. Chen, S.K. Sinha, A.N. Parikh, Long-range interlayer alignment of intralayer domains in stacked lipid bilayers, Nat. Mater. 11 (2012) 1074–1080, https://doi.org/10.1038/nmat3451.

[44] M. Kriechbaum, P. Laggner, States of phase transitions in biological structures, Prog. Surf. Sci. 51 (1996) 233–261, https://doi.org/10.1016/0079-6816(96)00003-2.

[45] B. Pozo Navas, K. Lohner, G. Deutsch, E. Sevcsik, K.A. Riske, R. Dimova, P. Garidel, G. Pabst, B.P. Navas, K. Lohner, G. Deutsch, E. Sevcsik, K.A. Riske, R. Dimova, P. Garidel, G. Pabst, Composition dependence of vesicle morphology and mixing properties in a bacterial model membrane system, Biochim. Biophys. Acta Biomembr. 1716 (2005) 40–48, https://doi.org/10.1016/j.bbamem.2005.08.003.

[46] A. Hickel, S. Danner-Pongratz, H. Amenitsch, G. Degovics, M. Rappolt, K. Lohner, G. Pabst, Influence of antimicrobial peptides on the formation of nonlamellar lipid mesophases, Biochim. Biophys. Acta Biomembr. 1778 (2008) 2325–2333, https://doi.org/10.1016/j.bbamem.2008.05.014.

[47] K. Hammond, M.G. Ryadnov, B.W. Hoogenboom, Atomic force microscopy to elucidate how peptides disrupt membranes, Biochim. Biophys. Acta Biomembr. 2021 (1863) 183447, https://doi.org/10.1016/j.bbamem.2020.183447.

[48] Y.S. Tarahovsky, A.L. Arsenault, R.C. MacDonald, T.J. McIntosh, R.M. Epand, Electrostatic control of phospholipid polymorphism, Biophys. J. 79 (2000) 3193–3200, https://doi.org/10.1016/S0006-3495(00)76552-0.

[49] A.T. Duran, H. Marbach, B. Rasul, K.L. Andrew Chan, R.D. Harvey, Fourier transform infrared spectroscopy detection of lipid ion-pairing in the Staphylococcus aureus plasma membrane, FASEB J. 30 (2016) 877.1.

[50] I.M. Hafez, S. Ansell, P.R. Cullis, Tunable pH-sensitive liposomes composed of mixtures of cationic and anionic lipids, Biophys. J. 79 (2000) 1438–1446, https://doi.org/10.1016/S0006-3495(00)76395-8.

[51] X.J. Li, M. Schick, Theory of tunable pH-sensitive vesicles of anionic and cationic lipids or anionic and neutral lipids, Biophys. J. 80 (2001) 1703–1711, https://doi.org/10.1016/S0006-3495(01)76141-3.

[52] K. Matsumoto, H. Hara, I. Fishov, E. Mileykovskaya, V. Norris, The membrane: transertion as an organizing principle in membrane heterogeneity, Front. Microbiol. 6 (2015) 572, https://doi.org/10.3389/fmicb.2015.00572.

[53] K. Matsumoto, J. Kusaka, A. Nishibori, H. Hara, Lipid domains in bacterial membranes, Mol. Microbiol. 61 (2006) 1110–1117, https://doi.org/10.1111/j.1365-2958.2006.05317.x.

[54] T.-H. Lee, V. Hofferek, M. Sani, F. Separovic, G. Reid, M.I. Aguilar, The impact of antibacterial peptides on bacterial lipid membranes depends on stage of growth, Faraday Discuss. (2020), https://doi.org/10.1039/d0fd00052c.

[55] S. Kuhn, C.J. Slavetinsky, A. Peschel, Synthesis and function of phospholipids in Staphylococcus aureus, Int. J. Med. Microbiol. 305 (2015) 196–202, https://doi.org/10.1016/j.ijmm.2014.12.016.

[56] I. Barák, K. Muchová, The role of lipid domains in bacterial cell processes, Int. J. Mol. Sci. 14 (2013) 4050–4065, https://doi.org/10.3390/ijms14024050.

[57] F. Grein, A. Müller, K.M. Scherer, X. Liu, K.C. Ludwig, A. Klöckner, M. Strach, H. Sahl, U. Kubitscheck, T. Schneider, Ca2+-daptomycin targets cell wall biosynthesis by forming a tripartite complex with undecaprenyl-coupled intermediates and membrane lipids, Nat. Commun. 11 (2020) 1455, https://doi.org/10.1038/s41467-020-15257-1.

[58] C. Slavetinsky, S. Kuhn, A. Peschel, Bacterial aminoacyl phospholipids – biosynthesis and role in basic cellular processes and pathogenicity, Biochim.

Biophys. Acta - Mol. Cell Biol. Lipids. 1862 (2017) 1310–1318, https://doi.org/10.1016/j.bbalip.2016.11.013.

[59] N. Ichihashi, K. Kurokawa, M. Matsuo, C. Kaito, K. Sekimizu, Inhibitory effects of basic or neutral phospholipid on acidic phospholipid-mediated dissociation of adenine nucleotide bound to DnaA protein, the initiator of chromosomal DNA replication, J. Biol. Chem. 278 (2003) 28778–28786, https://doi.org/10.1074/jbc.M212202200.

[60] T.H. Lee, V. Hofferek, F. Separovic, G.E. Reid, M.I. Aguilar, The role of bacterial lipid diversity and membrane properties in modulating antimicrobial peptide activity and drug resistance, Curr. Opin. Chem. Biol. 52 (2019) 85–92, https://doi.org/10.1016/j.cbpa.2019.05.025.